Modeling and simulation of a freight train brake system

Sajjad Sattari[1], Mohammad Saadat[1]*, Sayed Hasan Mirtalaie[1], Mehdi Salehi[1], Ali Soleimani[1]

[1]Department of Mechanical Engineering, Najafabad Branch, Islamic Azad University, Najafabad, Iran

ARTICLE INFO	A B S T R A C T
	The railway brake system is a very complex process with a great effect on traffic safety. This complexity originates from some different events in types of mechanical, electrical, thermal, etc that occur by braking. The main effective factors on performance and brake system function are braking force, speed of the vehicles, braking/stopping distance, condition of the railway, and environmental parameters. In this paper, a freight rail transportation system is modeled using a universal mechanism (UM). The under-analysis train includes two electric locomotives and 50 open wagons and the braking system is simulated in-service braking mode. First, the parameters of coupling force, braking force, brake cylinder pressure, braking distance, and speed (per initial speed of 30 m/s) were examined and evaluated, then the effect of friction coefficient (between wheel-pads) for different types of pads, maximum braking force, and maximum coupling force were evaluated. One of the results showed that application of two different materials, gray-iron, and composite, as a brake pad: (i) does not have a significant effect on the maximum coupling force, but (ii) the maximum braking force on the composite material in 1-2 wagons is about -120 kN and in 3-52 wagons is about -95 kN, while these values in gray-iron are about -40 kN and -28 kN for 1-2 wagons and 3-52 wagons, respectively.

1. Introduction

Due to the fact that freight trains are longer and heavier than passenger trains, there are more challenges to the brake system of these railway vehicles. Because of some important factors such as construction, design and operation, and technical features of vehicles, various braking systems have been developed. Two types of braking methods are used in railway vehicles: adhesion and non-adhesion braking. Fig. 1 also shows some examples of the operation of brake systems. For example, pneumatic disc-type or shoe-type brake systems are generally used for railway vehicles. Shoe brake devices are simple in design and have cost advantages. However, higher thermal loads due to high heavy loads

limit the optimal braking performance of this system. The disc braking systems provide smooth operations and low noise levels during braking as well as low maintenance costs. When brakes are applied, a special mechanism is used to reduce the rotational speed of the wheels. The mechanism can be pneumatically activated brake shoes or brake clamps [1-16]. As shown in Figure 1 (a), a compressor is placed on the locomotive in typical air brake systems to produce compressed air and store it in the main reservoir. The driver's control valve can select the options of charging compressed air from the main reservoir to the brake pipe or discharging the air into the brake pipe into the atmosphere. On individual wagons, the compressed air is stored in auxiliary reservoirs. As shown in Figure 1 (a), distributor valves determine the

---

*Corresponding author
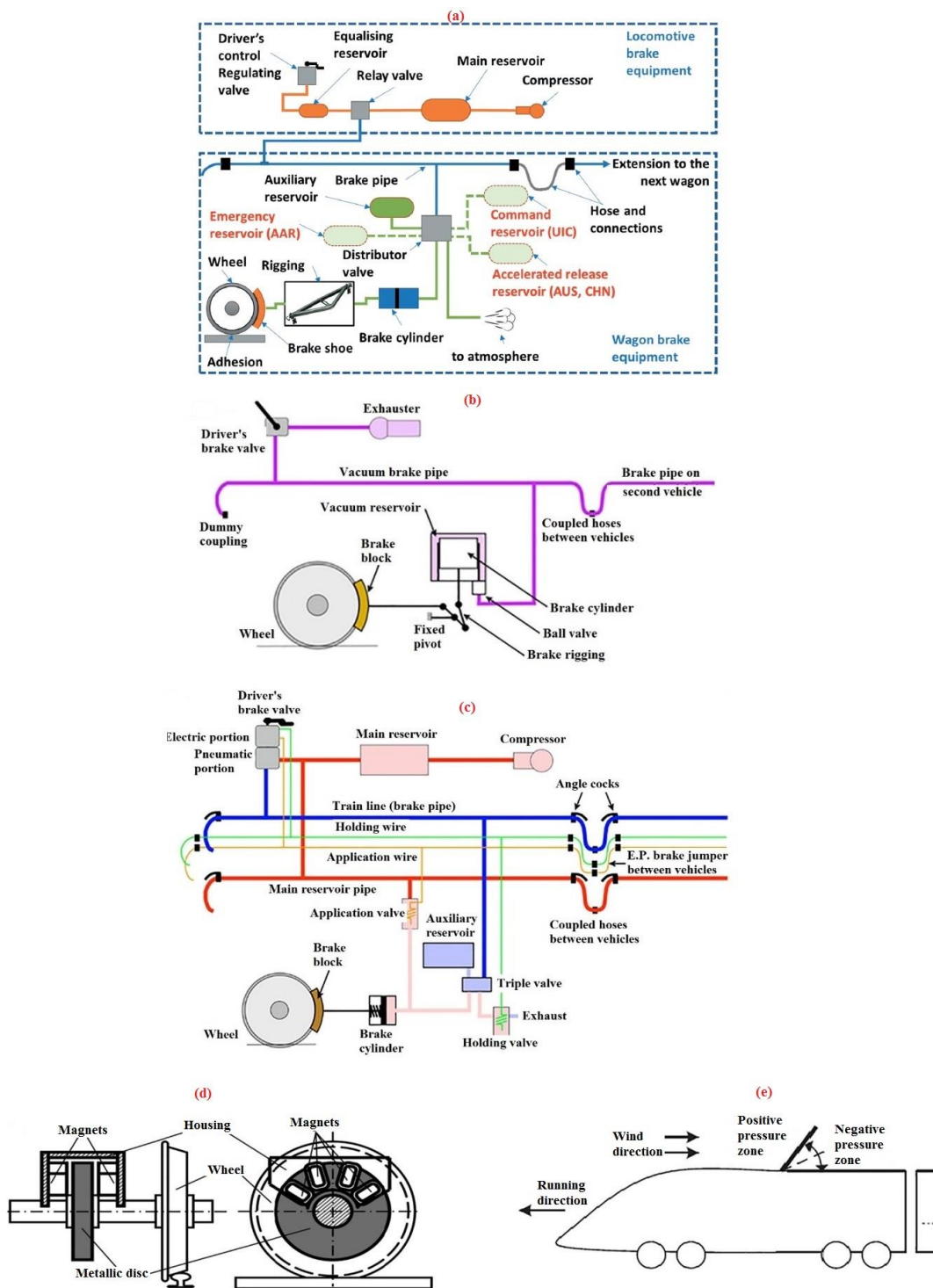Email address: mohammad.saadat.iaun@gmail.com

Figure 1. (a) Typical freight train air brake (b) vacuum brake system, (c) electro-pneumatic brake control,
(d) rotating eddy current braking (dynamic braking), and (e) aero-dynamic braking process

connection passages between auxiliary reservoirs, brake pipes, brake cylinders, and atmosphere.

During brake applications, compressed air flows from auxiliary reservoirs to brake cylinders and then presses the brake shoes against the wheel treads via brake riggings. During brake release, distributor valves let compressed air in brake cylinders discharge to the atmosphere so as to release the pressure on brake shoes [4].

Conventionally, train braking simulations were conducted under the topic of longitudinal train dynamics (LTD). In LTD, all vehicles are simplified as rigid bodies with single Degrees of Freedom (DOF). Wheel-rail contacts are neglected and only the longitudinal translation DOF is considered for each vehicle [16-24]. Wu et al. [16] simulated a train with the configuration of 1 locomotive +120 wagons +1 locomotive +120 wagons with three different braking scenarios: emergency brake, full-service brake, and minimum service brake.

Universal mechanism (UM) software is used for the simulation of both 3D rail vehicles and 1D trains for about two decades [25-30]. Pogorelov et al. [18] used the train 3D technique which is an efficient tool for the fast simulation of coupled 3D and 1D rail vehicle models in UM software. Comparison of their simulation and experimental results, vertical and lateral accelerations, brake cylinder pressure, etc. had a good agreement. Petrenko [29] used UM software to simulate railway dynamics and examined factors such as coupling forces, brake cylinder pressure, and train speed distribution. Alturbeh et al. [31] simulated the train brake system in low adhesion conditions using MATLAB/Simulink software. Wei et al. [32] studied a freight car air brake system, numerically and experimentally, and analyzed the pressures in the brake pipe, brake cylinder, etc. Cui et al. [33] performed dynamic modeling and simulation of urban subway vehicles. One of their results was the effect of acceleration on the braking force. Their results showed that, in general, the absolute value of braking force increased with increasing speed. Freight rail transport includes rails and trains to transport cargo. The vehicles used to carry goods on the railway are collectively referred to as freight wagons. The main types are auto-rack, box-car, gondola-car, center-beam, covered-hopper, tank-car, coil-car, flat-car, refrigerated box-car, and open-top hopper [30, 34].

In the geometric design of railway tracks and the evaluation of train curving performance, the extreme conditions induced by the brake operations should be taken into account. Li et al. [1] showed that by applying brake operations, the coupler longitudinal force will produce a lateral component, and the maximum value of the coupler lateral force in the 20,000 t train is larger than that in the 10,000 t train (trains pass through a sharp curve). Jiang et al. [2]

Comparised the curve negotiation properties of two different articulated monorail vehicles. Bosso et al. [3] explained that the in-train forces on curved track are higher than on straight track since the relative rotation between the wagons modifies the distance between the markers where the coupler is defined.

Air brakes are the most common type of brakes in railway operations; non-mainstream brake systems such as aero-dynamic, eddy-current and etc. brakes are not discussed in this work. Dynamic braking that uses traction motors as a part of the brake system is also outside of the scope. Note that air brake systems can vary significantly in different countries and regions. According to very limited studies in the field of brake systems simulation by software such as UM, in this paper, first, a freight train (2 locomotives +50 open wagons) is modeled, Then dynamic simulation in brake mode is proposed, and results are presented after simulating the macro-geometry of the track and determining the braking parameters. Finally, the coupling force and the maximum braking force for different types of brake pads (composite and gray-iron) are compared.

2. Modeling

Longitudinal train dynamics (LTD) is defined as the motions of rolling stock vehicles in the direction of the track (longitudinal). It, therefore, includes the motion of the train as a whole and any relative motions between vehicles. It is usually assumed that there is no lateral or vertical movement of the locomotives and wagons. Force inputs that are considered in conventional LTD include in-train force, traction force, dynamic brake force, air brake force, curving resistance, etc. The freight train model, simulated in this work in the UM software, is shown in Figure 2. This model consists of Russian two-section electric locomotive VL80s and 50 freight open wagons (similar to references [1, 17-18]). It is noteworthy that each locomotive and each wagon includes two bogies with 4 wheels installed on each bogie. Some specifications of locomotives, wagons, and gear Sh-2-T are given in Tables 1 and Figure 3. Many different draft gear models have been reported in the literature [35-44].
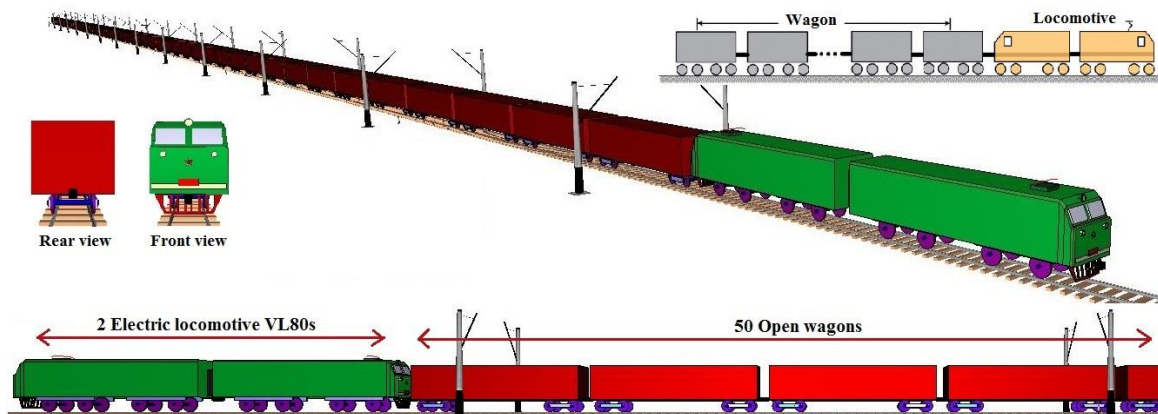
Figure 2. Simulated model in UM.

Table 1. Model key parameter.

Vehicle type	Locomotive	Open wagon
Vehicle mass (kg)	96000	90000
Vehicle length (m)	16.42	14.73
Wheel radius (m)	0.625	0.475
Distance between rail head and car-body bottom (m)	1.175	0.96
Distance between bogie centres (m)	7.5	10.53
Distance between wheel treads (m)	1.58	1.58
Distance between rail head and coupling axis (m)	1.05	1.05
Coupling length (m)	1	1
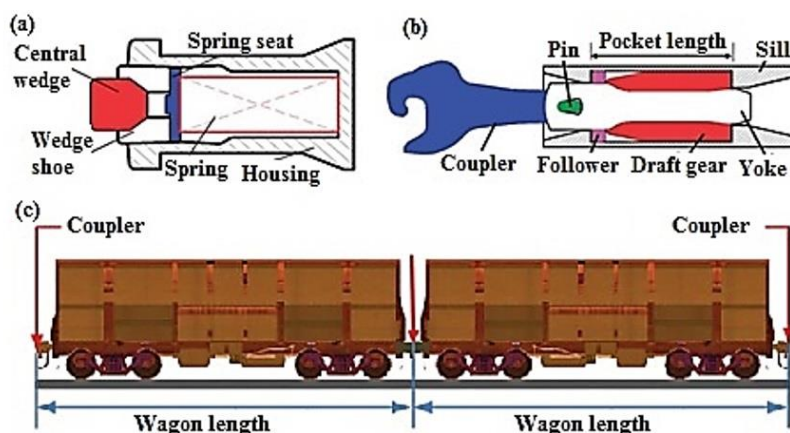
Draft gear, type: SH–2-T

Length (m)	Spring stifness (N/m)	Body stifness (N/m)	Work damping coefficient	Friction coefficient (main)	Friction coefficient (auxil.)
0.625	1.6e6	1e9	5e5	0.366	0.2

Figure 3. Typical fright coupler system: (a) draft gear, (b) coupler system assembly, and (c) wagon pair.

The model used in this paper has the structure shown in Fig. 3 and can be expressed as Eq. (1):

$$F_c = \frac{F_s \tan\varphi}{\tan\varphi \pm \mu} \qquad (1)$$

where F_c is the draft gear force; F_s is the spring force, φ is the wedge angle, and μ is the friction coefficient. More details of this draft gear model can be found in [40-41]. Wagon connection systems, are made up of two major groups: (i) coupler systems and (ii) buffer systems. Coupler systems are more widely used in Australia, America, Russia, and China while buffer systems are more widely used in Europe [4, 16, 18, 41].

3. Dynamic simulation

The service brake is a basic feature of any brake system, during which pressurized air flows from the auxiliary reservoir to the brake cylinder. Brakes can be applied at smaller pressure reductions and then moved to larger pressure reductions, i.e., graduated brakes [4]. In this paper, first modeling is performed and the parameters of coupling force, braking force, brake cylinder pressure, braking distance, and speed (per initial speed of 30 m/s) are investigated and then the effect of different friction coefficients between wheel-pads for different pad materials such as composite and gray-iron on maximum coupling force and maximum braking force is examined.

3.1. Solver parameters

Simulation process parameters for analyzing this model are as follows: solver: Park, type of solution: range space method (RSM), turn on the computation of the jacobian switch and set the simulation time (t): 50 (s) (the braking time will be about 50 s). It is noteworthy that in this work, an implicit multi-step method is considered as a solver, like the Park method, which has been used in several articles [17, 28, 26, 45]. In-solvable equations of traditional methods can be solved with the park method, a useful solver of the second order with variable step size, and a more complicated dynamic model could be built [45].

3.2. Track macro-geometry

The horizontal and vertical profiles of the railway track, are shown in Figure 4.

3.3. Resistance

In the list of loaded resistance force models by UM software, there are four standard models of train driving resistance forces for traveling on long welded rails. The resistance models used in this research and their related equations are presented in the appendix. It should also be noted that the resistance in the curve uses the force model according to Eq. 2 and the values are considered as follows:

$$W_r = \frac{a}{(R-b)} \qquad (2)$$

where W_r is a specific curving resistance force (N/t), a is a constant factor that is equal to 6116 according to recommendations from
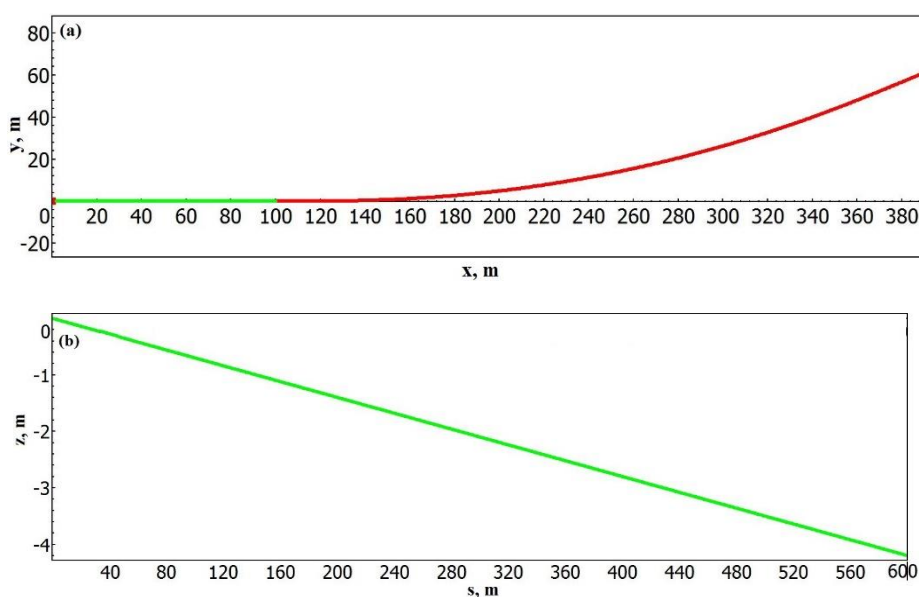

Figure 4. Railway track geometry: (a) horizontal profile, and (b) vertical profile.

(N.m/t), R is the radius of a curve (m), and b equals zero [3, 26, 46-47].

3.4. Braking system

The braking forces are essentially influenced by the friction coefficients involved, their dependence on different parameters having an important role in the braking characteristics of the vehicle. There are many factors determining the evolution of friction coefficients. Among them, the most important proved to be the running speed, the clamping forces, the surface contact pressure, and temperature. The friction coefficient between cast-iron braking shoes and wheel tread strongly depends on the instantaneous running speed, the applying force on each shoe, and the contact pressure, while the use of composite materials for brake shoes or pads enables independence of the friction coefficient on the mentioned parameters (Fig. 5 (a)) [13].

Having determined pressures in brake cylinders, the next step of brake simulation is to convert cylinder pressures to normal forces on brake shoes/pads and then to friction forces applied on wheels. The conversion from cylinder pressures to brake normal forces is achieved via brake rigging setups. A simplified diagram of

brake rigging is shown in Figure 5 (b) where a simple lever is used. In most brake simulations, friction forces generated from brake shoes (F_b in Fig. 5 (b)) is used as the brake forces with the assumption that wheel-rail adhesion can provide sufficient tangential forces in wheel–rail interfaces [4]. Martin et al. [5] calculated brake forces as (Eq. 3):

$$F_b = \frac{P_{b,t}}{P_{b,max}} \delta_{bm\%} m_{car} \delta_{total} \mu_b \qquad (3)$$

where $\delta_{bm\%}$ is the brake mass percentage; δ_{total} is the total efficiency of the brake system; and μ_b is the brake shoe coefficient of friction [4, 5].

The following parameters are necessary to set in creating the train brake system: friction coefficient between wheel and brake pad, type of braking modes (service, emergency, and release mode), brake rigging models, and speed of braking wave. Service braking is a type of adhesion brake and is done by using a disc brake and regenerative braking. However, emergency braking is completely accomplished by a pressurized air-driven disc brake [11-13]. In this paper, the type of brake is set in brake pipe mode in service braking mode. The brake force (FB) is defined as Eq. (4)
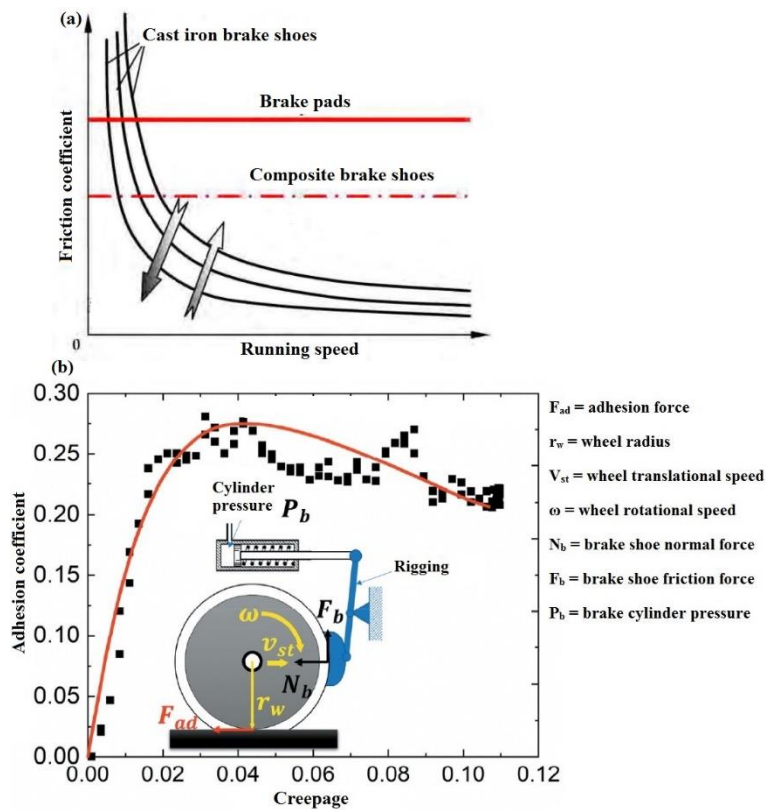

Figure 5. (a) friction coefficient for different braking systems, (b) Wheel/rail adhesion and brake systems.

$$F_B = f \cdot F_N \tag{4}$$

where f is the friction coefficient at the contact between the wheel and the brake pad, and F_N is the normal (loading) force at the contact between the wheel and the brake pad. Loading force and friction coefficient are calculated separately for every vehicle taking into account the number of friction pairs wheel pads. For this purpose, friction coefficient and loading force models are created and assigned to train vehicles. The friction coefficients mainly influence the braking forces. These coefficients are dependent on several parameters such as instantaneous running speed, applied/clamping force, contact surface pressures, and temperature. In the practical calculation, various empirical relations are obtained for the friction coefficient between the wheel and brake shoes [12-13], two of them are presented in Eq. (5) (UIC formula) [12-13] and Eq. (6) (Karvatzki formula) [13].

$$\mu_s(V, P_s) = 0.49 \frac{\frac{10}{3.6}V+100}{\frac{35}{3.6}V+100} \cdot \frac{\frac{875}{g}P_s+100}{\frac{2860}{g}P_s+100} \tag{5}$$

$$\mu_s(V, P_s) = 0.6 \frac{V+100}{5.V+100} \cdot \frac{\frac{16}{g}P_s+100}{\frac{86}{g}P_s+100} \tag{6}$$

were V is running speed (km/h), P_s is applied force on a brake shoe (kN), and g is gravitational acceleration 9.81 m/s^2.

4. Results and discussion

Air brake models have also been regarded as one of the most important components in LTD simulations as braking usually generates large in-train forces. Another motivation for brake studies is that brake applications usually generate large compressive in train forces which, from vehicle dynamics perspectives, pose higher risks than tensile forces on curves. Force inputs in a conventional LTD include coupling force, traction force, dynamic brake force, curving resistance, propulsion resistance, etc. [18]. Simulation results are presented in Figures 6 and 7. Figure 6(a) shows the coupling force (force in wagon connections), 6(b) braking force, 6(c) brake cylinder pressure, and figure 7(a) indicates the velocity of the first vehicle and 7(b) the vehicle distance (vehicle distance from the simulation start). The forces in wagon connections are shown in Figure 6(a). The maximal force is about 310 kN on the 37th vehicle. The plots of braking forces are presented in Figure 6(b). These values are about -120 kN for wagons 1 and 2 and about -95 kN for wagons 3-52. Figure 6(c) also shows the pressure behavior of the vehicle brake cylinder pressure. The brake cylinder pressure behavior diagram shown in Figure 6(c) is consistent with the results presented in the research of Wu et al. [16]. The results of numerical simulations and experiments by Wui et al. [32] showed that during the braking process, the pressure of the brake pipe in the first car decreases rapidly and the auxiliary tank pressure decreases thereafter. The brake cylinder is under pressure so that the piston starts to brake. When the pressure in the brake cylinder increases, there is a small pulse (shown as a platform in the curve) which indicates that most of the air pressure at this point is used to move the piston of the brake cylinder. When the brake cylinder piston is fully depressed, it resumes its increasing pressure to reach an equalizing pressure and similar behavior can be seen in Figure 6(c). The graph of the changes of the velocity of the first vehicle is shown in Figure 7 (a). The velocity of vehicle number 1 (locomotive number 1) starts from 30 m/s and reaches zero after about 48 seconds. Also, the traveled distance during this period is about 900 m, which can be seen in Figure 7(b).

There are four steps in the braking process, as follows [32]:

- First step (phase-1): It is considered from the braking command to reaching the brake release to the last air distributor of the train. During this step, the brakes are activated sequentially on the trains, and at the end of the first phase, the pressure is reached the maximum value, which corresponds to the brake cylinder pressure between the first and last vehicle of the train.

- Second step (phase-2): This phase starts from the end of the first phase until the command air pressure reaches the maximum value in the brake cylinders. During this period, the pressure increases uniformly in all brake cylinders.

- Third step (phase-3): It initiates from the end of the second phase and continues till reaching the maximum pressure in the brake cylinders of the last vehicle of the train. During this step, the maximum pressure occurs continuously in the brake cylinders.

- Fourth step (phase-4): It is considered from the end of the third phase to the train stop

or braking. As the maximum pressure in all brake cylinders is maintained during this stage, the braking forces are continuously maintained at their maximum values throughout the train and therefore the deformations are stopped. These steps are according to Ref. [13].
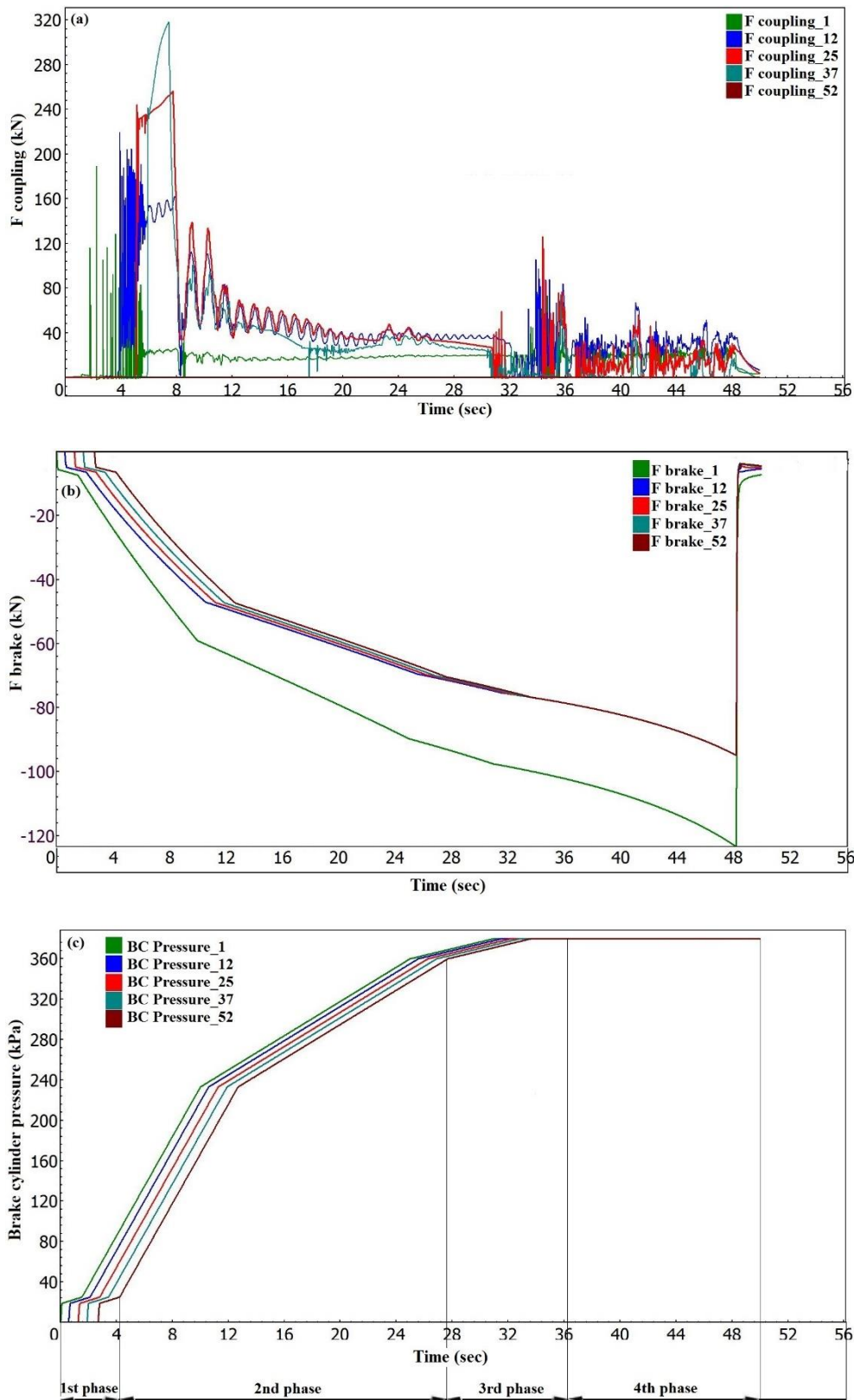

Figure 6. (a) coupling force, (b) braking force, and (c) brake cylinder pressure.
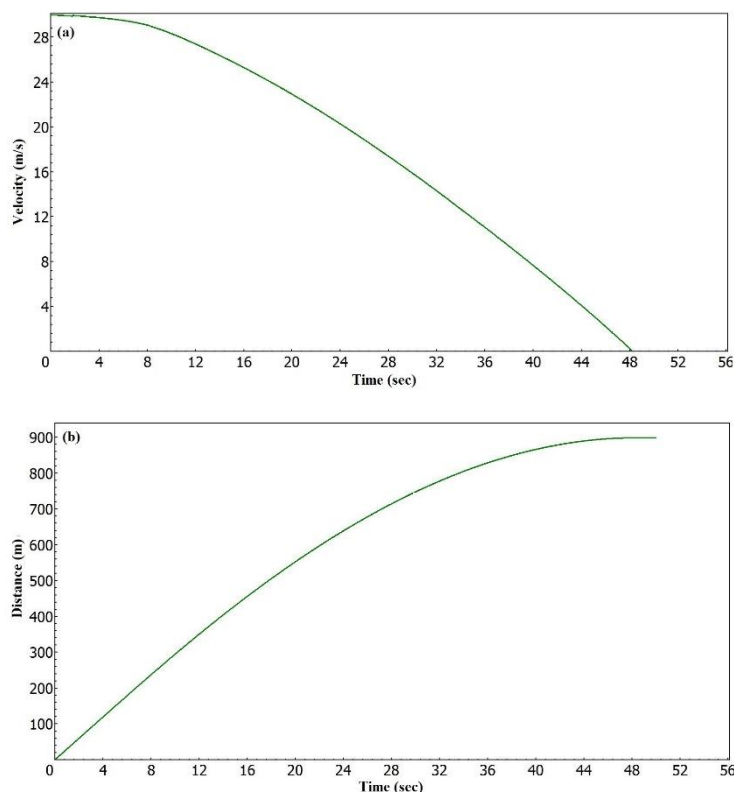
Figure 7. (a) velocity and (b) distance.

Figure 8 compares the maximum coupling force of wagons 1, 12, 25, 37, and 51 for two different pad materials of composite brake and gray-irons. It is noteworthy that the difference in coupling force values for two different types of pads for the same wagons is small. Also, the maximum braking force of all wagons for the two different materials of the composite pad and gray-iron is compared in Figure 9. The results show that the application of composite materials has the absolute maximum braking force compared to gray-iron. For example, the maximum braking force in the composite material in 1-2 wagons is about -120 kN, and in the 3-52 wagons it is about -95 kN, while the values in gray-iron material in the 1-2 wagons are about -40 kN and in wagons, 3-52 is about -28 kN.

Ghafelehbashi et al. [48] derived the mathematical model for the thermal modeling of a brake shoe in a railway vehicle. Their results showed that the maximum temperature in brake shoes occurred at the interface of the shoe and the wheel. Also, in both continuous and emergency braking modes, the temperature produced in composite brake shoes was lower

than that of the cast iron shoes. By increasing the velocity of the vehicle in continuous braking, the maximum temperature increased in both the composite and cast-iron brake shoes. It should be noted that the brake pads in braking systems are usually made of cast-iron and composite materials.

- Cast-iron with different grades is suitable due to metallurgical stability behavior. For example, GG25 has been used in the Y32 bogies for reasons such as high thermal conductivity, high thermal dissipation power, resistance to thermal loads, low cost, and ease of production.

- Composite materials: composites usually contain one or more materials as the matrix phase and one or more materials as the reinforcement phase. Based on the matrix phase, these materials are divided into the following 3 general groups: (i) polymer matrix composites (PMCs): in this category of materials, the base phase is a polymer (thermoplastic and/or thermoset) and the reinforcement phase is glass fiber, carbon, etc. Brake pads made with this method are usually easier and cheaper to produce compared to other composites, but they do not have good resistance to high temperatures; (ii)

metal matrix composites (MMCs): aluminum matrix metal composites (AMMCs) can be used in various industries, including the rail transportation industry, due to their high strength and rigidity, low-density, good wear resistance, and maintaining high-temperature properties; for example, Al-SiC and Fe-cu-based. These materials are made of two methods, solid-state processes and liquid-state processes that powder metallurgy (PM) process is one of these solid and suitable methods; (iii) ceramic matrix composites (CMCs): these materials have properties such as high-hardness, good-strength, good-corrosion resistance, etc .; however, due to

their inherent fragility, the use of these materials has been limited so far [12-13, 49-51].

5. Conclusions

It is widely acknowledged that modelling of wagon connection systems and air brake systems are two major challenges for modelling of LTD. Due to the numerous dynamic rail simulations of researchers with the help of UM software and very little attention to the issue of braking, in this work, an attempt has been made to address this issue. In the first step, modeling of a freight rail transportation system (2 locomotives +50 open
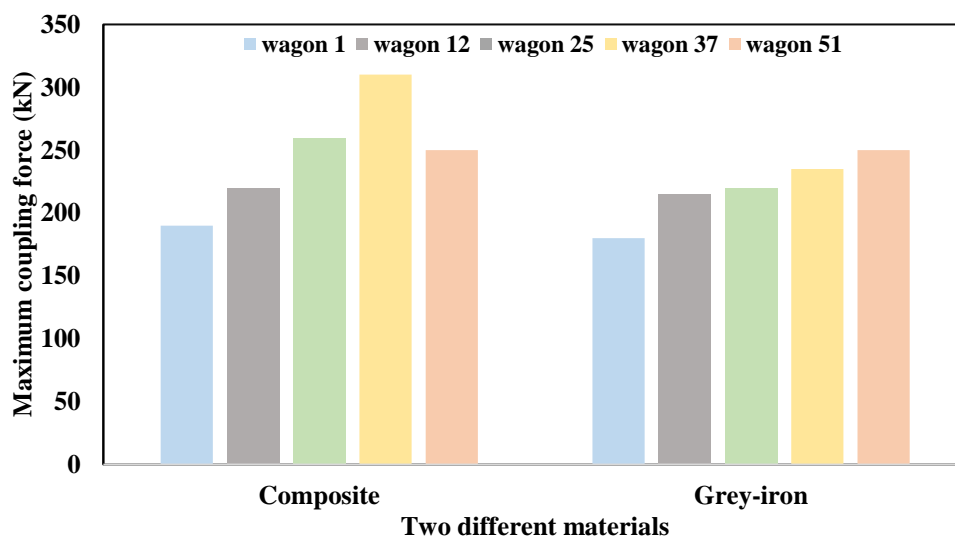

Figure 8. Absolute value of the maximum coupling force for two different materials.
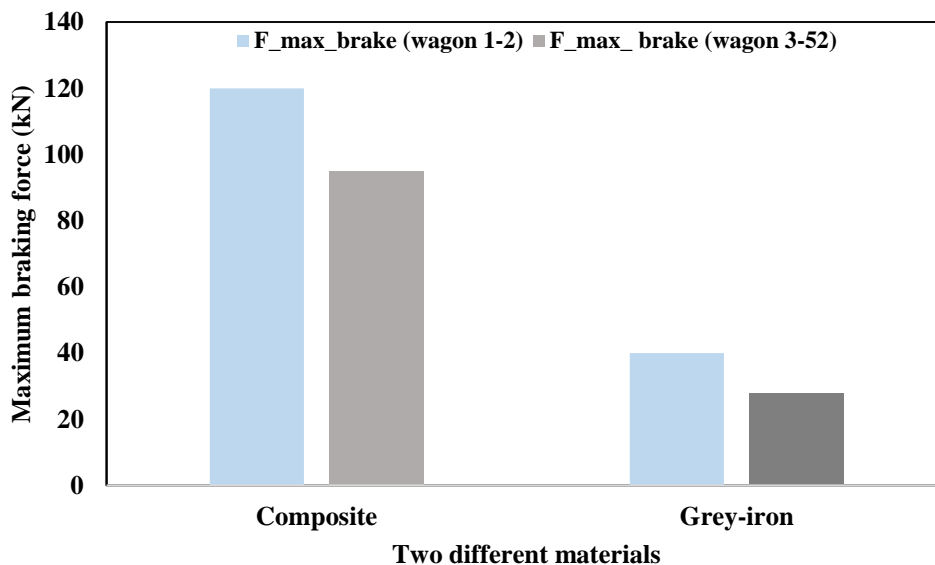

Figure 9. Maximum braking force for two different materials.

wagons) was done with UM software. In the next step, by entering the designed model into the UM simulation environment, a braking system was defined and the results were presented.

For this purpose, first, the parameters of coupling force, braking force, cylinder pressure, distance traveled and speed for the initial speed of 30 m/s have been investigated and evaluated. One of the results of these studies showed that the behavior of the brake cylinder pressure diagram was in good agreement with other studies. Then, the effect of the friction coefficient between the wheel-pad for different materials of the brake pad, on the maximum braking force and the maximum coupling force was evaluated. The results of this study showed that the application of two different materials, gray-iron, and composite: (i) does not have a significant effect on the maximum coupling force, but (ii) the maximum braking force in the composite material was about -120 kN for wagons 1 and 2, and about -95 kN for wagons 3-52, while values in iron material were about -40 kN in wagons 1and 2, and about -28 kN in wagons 3-52.

References

[1] Liu, P. and Wang, K. 2017. Effect of braking operation on wheel–rail dynamic interaction of wagons in sharp curve. Proc IMechE Part K: J Multi-body Dynamics. 231(1): 252–265.

[2] Jiang, Y., Wu, P., Zeng, J. and Gao, H. 2018. Comparison of the curve negotiation properties of two different articulated monorail vehicles. Proc IMechE Part F: J Rail and Rapid Transit. 0(0): 1–13.

[3] Bosso, N., Gugliotta, A. and Zampieri, N. 2018. A mixed numerical approach to evaluate the dynamic behavior of long trains. Procedia Structural Integrity. 12: 330-343.

[4] Wu et al. 2021. Freight train air brake models. International Journal of Rail Transportation.

[5] Martin GC. and Hay WW. 1967. Method of analysis for determining the coupler forces and longitudinal motion of a long freight train. Urbana (IL): University of Illinois

[6] Sattari, S., Saadat, M., Mirtalaie, SH., Salehi, M., Soleimani, A. 2022. Estimation and evaluation of wheel/rail dynamic forces in railway tracks- numerical study. 2nd International Conference on Computer Engineering and Science (CCES).

[7] Sattari, S., Saadat, M., Mirtalaie, SH., Salehi, M., Soleimani, A. 2022. Modeling a passenger train and analyzing the ride comfort in different conditions with the Sperling index. 2nd International Conference on Computer Engineering and Science (CCES).

[8] Sattari, S., Saadat, M., Mirtalaie, SH., Salehi, M., Soleimani, A. 2023. Evaluation of Sperling's index in passenger and freight trains under different speeds and track irregularities. International Journal of Advanced Design and Manufacturing Technology (ADMT), DOI: 10.30486/admt.2023.1963242.1367.

[9] Sattari, S., Saadat, M., Mirtalaie, SH., Salehi, M., Soleimani, A. 2023. Effects of train speed, track irregularities, and wheel flat on wheel-rail dynamic force. International Journal of Heavy Vehicle Systems. In Production.

[10] Sattari, S., Saadat, M., Mirtalaie, SH., Salehi, M., Soleimani, A. 2023. Parametric study of wheel flats effects on dynamic forces and derailment coefficient in turnouts. International Journal of Heavy Vehicle Systems. In Production.

[11] Cruceanu, C. and Crăciun, C. 2018. Aspects regarding braking process of passenger trains with different braking systems in composition. IOP Conference Series: Materials Science and Engineering. 400: 042012.

[12] Günay, M., Korkmaz, M.E. and Özmen, R. 2020. An investigation on braking systems used in railway vehicles. Engineering Science and Technology, an International Journal. 23(2): 421-431.

[13] Cruceanu, C. 2012. Train braking, reliability and safety in railway. ed. InTech, China.

[14] Krishna, V.V., Jobstfinke, D., Melzi, S. and Berg, M. 2021. An integrated numerical framework to investigate the running safety of overlong freight trains. Proceedings of the Institution of Mechanical Engineers, Part F: Journal of Rail and Rapid Transit. 235(1): 47-60.

[15] Ridolfi, A., Vettori, G., Allotta, B., Pugi, L., Malvezzi, M. and Rindi, A. 2011. A multibody model of a railway vehicle for the development of innovative odometry systems. ed.

[16] Wu, Q., Cole, C. and Spiryagin, M. 2020. Train braking simulation with wheel-rail adhesion model. Vehicle System Dynamics. 58(8): 1226-1241.

[17] Wu, Q., Spiryagin, M., Cole, C., Chang, C., Guo, G., Sakalo, A., Wei, W., Zhao, X., Burgelman, N., Wiersma, P., Chollet, H., Sebes, M., Shamdani, A., Melzi, S., Cheli, F., di Gialleonardo, E., Bosso, N., Zampieri, N., Luo, S., Wu, H. and Kaza, G.-L. 2018. International benchmarking of longitudinal train dynamics simulators: Results. Vehicle System Dynamics. 56(3): 343-365.

[18] Spiryagin, M., Wu, Q. and Cole, C. 2017. International benchmarking of longitudinal train dynamics simulators: Benchmarking questions. Vehicle System Dynamics. 55(4): 450-463.

[19] AmberbirWondimu, Negash Alemu, Yohanes Regassa and, P. Sivaprakasam. 2020. Modelling and simulation of effect of missed bolt on rail end joint by fem. International Journal of Ambient Energy.

[20] Cheli, F., Di Gialleonardo, E. and Melzi, S. 2017. Freight trains dynamics: Effect of payload and braking power distribution on coupling forces. Vehicle System Dynamics. 55(4): 464-479.

[21] Cantone, L. 2011. Traindy: The new union internationale des chemins de fer software for freight train interoperability. Proceedings of the Institution of Mechanical Engineers, Part F: Journal of Rail and Rapid Transit. 225(1): 57-70.

[22] Sun, Y., et al., Longitudinal heavy haul train simulations and energy analysis for typical Australian track routes. 2013. Proceedings of the Institution of Mechanical Engineers, Part F: Journal of Rail and Rapid Transit. 228(4): 355-366.

[23] Wu, Q., Spiryagin, M. and Cole, C. 2016. Longitudinal train dynamics: An overview. Vehicle System Dynamics. 54(12): 1688-1714.

[24] Jackiewicz, J. 2021. Coupler force reduction method for multiple-unit trains using a new hierarchical control system. Railway Engineering Science. 29(2): 163-182.

[25] Sładkowski, A. 2005. Rail vehicle dynamics and associated problems. ed. Silesian University of Technology.

[26] Kovalev, R., Sakalo, A., Yazykov, V., Shamdani, A., Bowey, R. and Wakeling, C.

2016. Simulation of longitudinal dynamics of a freight train operating through a car dumper. Vehicle System Dynamics. 54(6): 707-722.

[27] Pogorelov, D. and Yazykov, V. 2009. Computer simulation of train dynamics. Multibody Dynamics.): 392-393.

[28] Pogorelov, D., Yazykov, V., Lysikov, N., Oztemel, E., Arar, O.F. and Rende, F.S. 2017. Train 3d: The technique for inclusion of three-dimensional models in longitudinal train dynamics and its application in derailment studies and train simulators. Vehicle System Dynamics. 55(4): 583-600.

[29] Petrenko, V. 2016. Simulation of railway vehicle dynamics in universal mechanism software. Procedia Engineering. 134: 23-29.

[30] Gao, M., Cong, J., Xiao, J., He, Q., Li, S., Wang, Y., Yao, Y., Chen, R. and Wang, P. 2020. Dynamic modeling and experimental investigation of self-powered sensor nodes for freight rail transport. Applied Energy. 257: 113969.

[31] Alturbeh, H., Stow, J., Tucker, G. and Lawton, A. 2020. Modelling and simulation of the train brake system in low adhesion conditions. Proceedings of the Institution of Mechanical Engineers, Part F: Journal of Rail and Rapid Transit. 234(3): 301-320.

[32] Wei, W. and Lin, Y. 2009. Simulation of a freight train brake system with 120 valves. Proceedings of the Institution of Mechanical Engineers, Part F: Journal of Rail and Rapid Transit. 223(1): 85-92.

[33] Cui, X., Zou, R., Gu, M. and Zou, Y. 2020. Urban subway vehicle dynamic modelling and simulation. IOP Conference Series: Materials Science and Engineering. 719: 012042.

[34] Xie, C., Tao, G., Liang, S. and Wen, Z. 2021. Understanding and treatment of brake pipe fracture of metro vehicle bogie. Engineering Failure Analysis. 128: 105614.

[35] Wu, Q., Cole, C., Luo, S. and Spiryagin, M. 2014. A review of dynamics modelling of friction draft gear. Vehicle System Dynamics. 52(6): 733-758.

[36] Olshevskiy, A., Olshevskiy, A., Kim, C.-W. and Yang, H.-I. 2018. An improved dynamic model of friction draft gear with a transitional characteristic accounting for housing

deformation. Vehicle System Dynamics. 56(10): 1471-1491.

[37] Wu, Q., Luo, S., Qu, T. and Yang, X. 2017. Comparisons of draft gear damping mechanisms. Vehicle System Dynamics. 55(4): 501-516.

[38] Serajian, R., Mohammadi, S. and Nasr, A. 2019. Influence of train length on in-train longitudinal forces during brake application. Vehicle System Dynamics. 57(2): 192-206.

[39] Cole, C., Spiryagin, M., Wu, Q. and Sun, Y.Q. 2017. Modelling, simulation and applications of longitudinal train dynamics. Vehicle System Dynamics. 55(10): 1498-1571.

[40] Iwnicki, S. 2006. Handbook of railway vehicle dynamics. ed. CRC press.

[41] Wu, Q., Cole, C., Spiryagin, M. and Ma, W. 2018. Preload on draft gear in freight trains. Proceedings of the Institution of Mechanical Engineers, Part F: Journal of Rail and Rapid Transit. 232(6): 1615-1624.

[42] Cole, C. and Sun, Y.Q. 2006. Simulated comparisons of wagon coupler systems in heavy haul trains. Proceedings of the Institution of Mechanical Engineers, Part F: Journal of Rail and Rapid Transit. 220(3): 247-256.

[43] Wu, Q., Luo, S., Xu, Z. and Ma, W. 2013. Coupler jackknifing and derailments of locomotives on tangent track. Vehicle System Dynamics. 51(11): 1784-1800.

[44] Wu, Q., Spiryagin, M. and Cole, C. 2014. A dynamic model for friction draft gear. ed.

[45] Jiang, Y., Wu, P., Zeng, J., Wu, X., He, Q. and Wang, X. 2021. Influence of bridge parameters on monorail vehicle–bridge system— a research with multi-rigid body and multi-flexible body coupling theory and park method. Journal of Low Frequency Noise, Vibration and Active Control. 40(3): 1194-1214.

[46] Cole, C. 2006. Longitudinal train dynamics. Handbook of railway vehicle dynamics.): 239-278.

[47] Wu, Q., Spiryagin, M. and Cole, C. 2020. Train energy simulation with locomotive adhesion model. Railway Engineering Science. 28(1): 75-84.

[48] Ghafelehbashi, SME. and Talaee MR. 2021. An analytical thermal model of a railway vehicle brake shoe. Proc IMechE Part F: J Rail and Rapid Transit. 0(0): 1–11.

[49] Pradnya Kosbe, Pradeep Patil, and Rajendra Kulkarni. 2020. Fade and recovery characteristics of commercial disc brake friction materials: a case study. International Journal of Ambient Energy.

[50] Sattari, S., Jahani, M., Atrian, A. 2017. Effect of Volume Fraction of Reinforcement and Milling Time on Physical and Mechanical Properties of Al7075–SiC Composites Fabricated by Powder Metallurgy Method. Powder Metallurgy and Metal Ceramics. 283-292.

[51] Sattari, S. and Jahani, M. 2017. An investigation of parameters involved and defects in the fabrication of Al–SiC nanocomposite using hot extrusion technique. Transactions of the Indian Institute of Metals. 2361-2370.

Appendix:

Resistnce model, locomotive	9.81*(2.4+0.009*v*3.6+0.00035*(v*3.6)*(v*3.6))*M/1000
Resistnce model, open wagon	9.81*(0.7*M/1000+(3+0.09*v*3.6+0.002*(v*3.6)*(v*3.6))*4)
Friction coefficient, composite	with main; name="Composite;" comment="Composite brake shoes;" with brakecoef; coefmode=2; coefexpression="0.44*(f/1000/9.8+20)/(4*f/1000/9.8+20)*(3.6*v+150)/(2*3.6*v+150) "; with end;
Friction coefficient, grey-iron	with main; name="Grey iron;" comment="Grey iron brake shoes;" with brakecoef; coefmode=2; coefexpression="0.6*(16*f/1000/9.8+100)/(80*f/1000/9.8+100)*(3.6*v+100)/(5*3.6*v+100) "; with end;